Displaced Path Integral Formulation for the Momentum Distribution of Quantum Particles

Lin Lin,[1] Joseph A. Morrone,[2,*] Roberto Car,[2,3,†] and Michele Parrinello[4]

[1]*Program in Applied and Computational Mathematics, Princeton University, Princeton, New Jersey 08544, USA*
[2]*Department of Chemistry, Princeton University, Princeton, New Jersey 08544, USA*
[3]*Department of Physics, Princeton University, Princeton, New Jersey 08544, USA*
[4]*Computational Science, Department of Chemistry and Applied Biosciences, ETH Zurich, USI Campus,
Via Giuseppe Buffi 12, CH-6900 Lugano, Switzerland*

The proton momentum distribution, accessible by deep inelastic neutron scattering, is a very sensitive probe of the potential of mean force experienced by the protons in hydrogen-bonded systems. In this work we introduce a novel estimator for the end-to-end distribution of the Feynman paths, i.e., the Fourier transform of the momentum distribution. In this formulation, free particle and environmental contributions factorize. Moreover, the environmental contribution has a natural analogy to a free energy surface in statistical mechanics, facilitating the interpretation of experiments. The new formulation is not only conceptually but also computationally advantageous. We illustrate the method with applications to an empirical water model, *ab initio* ice, and one dimensional model systems.

The behavior of protons and more generally of light nuclei in condensed phases is significantly affected by quantum effects even at ambient temperatures. The isotopic effect in water, the ferroelectric behavior of potassium diphosphate, and the formation of high pressure ice phases, are just a few of the relevant phenomena where the quantum behavior of the nuclei plays a role. To address these issues a powerful experimental tool, deep inelastic neutron scattering (DINS) that measures the momentum distribution [1–3] has recently been developed. Quantum effects are revealed by strong deviations from the classical Maxwell distribution. However, interpreting DINS experiments is difficult and so far has been based on extensive and challenging *ab initio* molecular dynamics simulations [4,5]. While these calculations have shown that good agreement between theory and experiments is possible, a simpler way of calculating the momentum distribution needs to be found and the link between the experimental data and the underlying physics made transparent if DINS is to become a standard tool.

In order to understand the source of this computational challenge, let us contrast the expression for the momentum distribution $n(\mathbf{p})$ and that of the partition function Z in terms of the density matrix $\rho(\mathbf{r}, \mathbf{r}') = \langle \mathbf{r} | e^{-\beta H} | \mathbf{r}' \rangle$. The former may be expressed as

$$n(\mathbf{p}) = \frac{1}{(2\pi\hbar)^3 Z} \int d\mathbf{r} d\mathbf{r}' e^{i/\hbar \mathbf{p}\cdot(\mathbf{r}-\mathbf{r}')} \rho(\mathbf{r}, \mathbf{r}')$$

$$= \frac{1}{(2\pi\hbar)^3} \int d\mathbf{x} e^{i/\hbar \mathbf{p}\cdot\mathbf{x}} \tilde{n}(\mathbf{x}), \tag{1}$$

where $\tilde{n}(\mathbf{x}) = \frac{1}{Z} \int d\mathbf{r} d\mathbf{r}' \delta(\mathbf{r} - \mathbf{r}' - \mathbf{x})\rho(\mathbf{r}, \mathbf{r}')$. The partition function is given by

$$Z = \int d\mathbf{r}\rho(\mathbf{r}, \mathbf{r}). \tag{2}$$

It can be seen that $n(\mathbf{p})$ involves the off-diagonal matrix elements while Z is determined solely by diagonal terms. In a condensed system the potential energy surface in which the particles move is in a high dimensional space and statistical sampling is the only viable computational strategy. This is usually done using the Feynman path representation. In this representation, $\tilde{n}(\mathbf{x})$ is an end-to-end distribution of a sum over open paths, while closed ones determine Z [6,7]. Sampling is done on the closed paths that specify Z and it is challenging from these simulations to estimate the open path distribution that determines $n(\mathbf{p})$.

One approach is to artificially open a fraction of the paths [8]. In so doing one has to balance two contradictory requirements. On one hand the number of open paths has to be large enough to obtain good statistics for $\tilde{n}(\mathbf{x})$, while on the other hand it cannot be too large as the sampling will become incorrect. In this work we introduce a new expression for $\tilde{n}(\mathbf{x})$ which does not require opening the paths and compromises neither sampling accuracy nor statistics. Following a derivation whose detail can be found in the supplementary material [9] we find

$$\tilde{n}(\mathbf{x}) = \tilde{n}_0(\mathbf{x})$$
$$\times \frac{\int \mathfrak{D}\mathbf{r}(\tau)\exp(-\frac{1}{\hbar}\int_0^{\beta\hbar} d\tau(\frac{m\dot{\mathbf{r}}^2(\tau)}{2} + V[\mathbf{r}(\tau) + y(\tau)\mathbf{x}]))}{\int \mathfrak{D}\mathbf{r}(\tau)\exp(-\frac{1}{\hbar}\int_0^{\beta\hbar} d\tau(\frac{m\dot{\mathbf{r}}^2(\tau)}{2} + V[\mathbf{r}(\tau)]))},$$
$$\tag{3}$$

where $\tilde{n}_0(\mathbf{x}) = e^{-(m\mathbf{x}^2/2\beta\hbar^2)}$ is the free particle end-to-end distribution. The function $y(\tau)$ is arbitrary but for the boundary condition $y(\beta\hbar) - y(0) = 1$. In practice, the optimal choice is to take $y = \frac{1}{2} - \frac{\tau}{\beta\hbar}$ since it minimizes the distance between $\mathbf{r}(\tau)$ and the displaced path $\mathbf{r}(\tau) + y(\tau)\mathbf{x}$. Notice that, for simplicity, Eq. (3) refers to a single particle

subject to the external potential $V[\mathbf{r}]$. Generalization to many-body systems is straightforward if exchange effects between identical particles can be neglected. How to include such effects will be discussed in a future publication. Equation (3) merits further comment. In the calculation of the kinetic energy it has been found to be extremely useful to use estimators in which the free particle contribution has been explicitly accounted for [10]. We expect similar computational advantages from the explicit separation of $\tilde{n}_0(\mathbf{x})$. Furthermore it follows from Eq. (3) that, having put $Z(\mathbf{0}) = Z$, we can write $\frac{\tilde{n}(\mathbf{x})}{\tilde{n}_0(\mathbf{x})} = \frac{Z(\mathbf{x})}{Z(\mathbf{0})}$ as a ratio between two partition functions. To calculate this ratio or its logarithm $U(\mathbf{x}) = -\ln\frac{Z(\mathbf{x})}{Z(\mathbf{0})}$ standard statistical mechanics methods such as free energy perturbation [11] or thermodynamic integration [12] may be utilized.

Using free energy perturbation one may compute

$$U(\mathbf{x}) = -\ln\langle e^{-(1/\hbar)\int_0^{\beta\hbar} d\tau (V[\mathbf{r}(\tau)+y(\tau)\mathbf{x}]-V[\mathbf{r}(\tau)])}\rangle_0, \quad (4)$$

where the average is evaluated using the closed path distribution $Z(\mathbf{0})$.

The free energy perturbation method can only be applied to systems with weak quantum effects. For systems with strong quantum effects the average is difficult to converge and instead we use thermodynamic integration. In this scheme $U(\mathbf{x})$ is obtained as an integral $U(\mathbf{x}) = \int_0^{\mathbf{x}} d\mathbf{x}' \cdot \mathbf{F}(\mathbf{x}')$ over the mean force,

$$\mathbf{F}(\mathbf{x}') = \left\langle \frac{1}{\hbar} \int_0^{\beta\hbar} d\tau \nabla_{\mathbf{r}} V[\mathbf{r}(\tau) + y(\tau)\mathbf{x}'] y(\tau) \right\rangle_{\mathbf{x}'} \quad (5)$$

evaluated at the intermediate distributions $Z(\mathbf{x}')$. In this case thermodynamic integration requires opening the paths, but it does so in a fully controlled way. Besides being rigorous our estimator offers several computational advantages. In three dimensions the standard approach suffers from poor statistics at short distances due to the geometrical r^2 factor, and this is not the case here. By averaging over all the particles, statistics can be greatly improved. The calculation over different particles is intrinsically parallel and the power of modern computers optimally harnessed. Furthermore, in crystals where anisotropies are relevant, the dependence of $n(\mathbf{p})$ on the momentum direction can be easily evaluated.

We first test our algorithm on a flexible model for water [13]. The simulation box contains 32 water molecules. The temperature is set to be 296 K. Both protons and oxygens are treated by quantum mechanics, and are represented by 64 classical beads. The end-to-end distribution is spherically averaged in water. The quantum effect for water at room temperature is relatively small [4]. This allows us to use free energy perturbation (4) and compare the results with open path integral simulation [8]. In the latter case, in principle one proton path should be opened and all other paths should be closed. However, the resulting statistics would be poor. In order to boost statistics one proton path

per water molecule was opened, as it was found that this approximation leads to a negligible error in the momentum distribution due to the relatively weak interaction between protons belonging to different water molecules [8]. The closed path formulation allows one to compute the end-to-end distribution without opening any proton path, and therefore all the protons can be included in the calculation of the end-to-end distribution without any approximation. We show the end-to-end distribution calculated both from a 268 ps open path simulation and from a 12 ps closed path simulation that utilizes the estimator given by Eq. (4) in Fig. 1(a), and the comparison of the potential of mean force in Fig. 1(b). In both simulations, the time step is 0.24 fs. Two consecutive steps contain highly correlated information, and the free energy perturbation estimator may be computed every 20 steps. Thus with only a small increase in computational overhead in comparison to an open path simulation of the same length, the displaced path formulation has a large gain in terms of sampling this property efficiently.

The thermodynamic integration approach given in Eq. (5) is not only computationally advantageous but also provides one with the potential of mean force $U(\mathbf{x})$, and its gradient $\mathbf{F}(\mathbf{x})$ which are key quantities for interpreting the physics underlying $n(\mathbf{p})$. We first note that the kinetic energy K is given by $K = \frac{\hbar^2}{2m}\nabla \cdot \mathbf{F}(\mathbf{x})|_{\mathbf{x}=\mathbf{0}} + \frac{3}{2\beta} \equiv K_V + \frac{3}{2\beta}$. Since $3/2\beta$ is the free particle contribution, the nonclassical contribution is completely included in the excess kinetic energy term K_V, and is determined by the zero point curvature of $U(\mathbf{x})$. Second, if the momentum distribution of an individual particle is accessible (as is possible, e.g., in simulations) and the underlying potential energy surface is harmonic, the end-to-end distribution follows a Gaussian distribution and the mean force is given by a
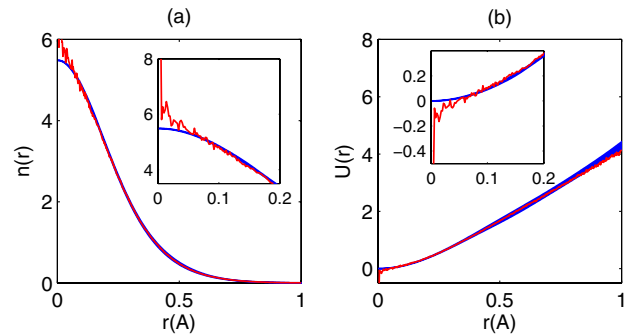

FIG. 1 (color online). Comparison of (a) the end-to-end distribution and (b) the potential of mean force in SPC/F2 water. In both (a) and (b), the red oscillatory line is computed by a 268 ps open path integral simulation. The blue smooth line is calculated using the displaced path estimator (4), with the thickness indicating the 95% confidence interval. The noise near $r = 0$ in both insets for open path simulation is due to the r^2 weight in the spherical integration, while the displaced path gives correct small r behavior by definition.

straight line. Any deviation of $\hat{\mathbf{q}} \cdot \mathbf{F}(\mathbf{x})$ from linearity signals anharmonic behavior along the $\hat{\mathbf{q}}$ direction.

In experiments, the spherically averaged momentum distribution is accessible in liquids, and amorphous and polycrystalline solids, while the directional distribution is also accessible in monocrystalline materials. The latter distribution provides more information about the underlying potential energy surface. However, in single crystals the total momentum distribution is the sum of the contributions of individual particles participating in bonds with different orientations. As a consequence the difference between directional and spherical momentum distribution is usually very small as shown in the top panel of Fig. 2. This figure is based on an anisotropic harmonic model [14] with three distinct principal frequencies that is fit to the *ab initio* path integral data for ice I*h* [4]. The bottom panel of the same figure clearly shows that the distinction between the spherical and directional distributions is enhanced when comparing the mean forces. It is therefore of great interest to link directly the mean force to the experimental data, i.e., to the Compton profile $J(\hat{\mathbf{q}}, y) = \int n(\mathbf{p})\delta(y - \mathbf{p} \cdot \hat{\mathbf{q}})d\mathbf{p}$ where $\hat{\mathbf{q}}$ indicates the direction of the neutron detector [2]. One finds with a derivation provided in the supplemental material [9] that the mean force is related to the Compton profile by

$$\hat{\mathbf{q}} \cdot \mathbf{F}(x\hat{\mathbf{q}}) = -\frac{mx}{\beta\hbar^2} + \frac{\int_0^\infty dy\, y \sin(xy/\hbar)J(\hat{\mathbf{q}}, y)}{\hbar \int_0^\infty dy \cos(xy/\hbar)J(\hat{\mathbf{q}}, y)}. \quad (6)$$

In the bottom panel of Fig. 2 the slope of the mean force, either spherical or directional, at $r = 0$ is equal to the
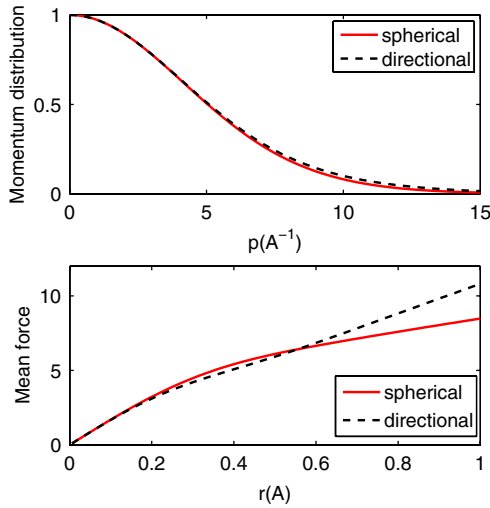
excess kinetic energy K_V divided by the constant $\frac{\hbar^2}{2m}$. This is an exact result that originates from the symmetry property of ice I*h*. In general the spherical and directional mean force can have different slopes at $r = 0$. The deviation of the spherical and directional forces from linearity at finite r results from the averaging process and is not a sign of anharmonicity. Thus in the interpretation of the experimental Compton profile, which results from the contribution of many particles, one must distinguish the case of an anisotropic harmonic potential energy surface from that of an anharmonic potential energy surface. To the best of our knowledge the procedure that is currently adopted to fit the experimental data [2,3,15] does not separate well anisotropic and anharmonic effects. We propose here an alternative approach in which the mean force is associated to the experimental Compton profile according to Eq. (6). The projections of the mean force along different directions are then fitted to an anisotropic harmonic model averaged as required by the crystal symmetry. Any systematic deviation from experiment of the mean force originating from the harmonic contribution, can then be associated with anharmonicity and used to further refine the underlying model potential energy surface.

The framework introduced here may be also utilized to provide insight to the investigation of anharmonic systems. Consider, for example, a particle with the proton mass

FIG. 2 (color online). Top panel: the momentum distribution of the protons in ice I*h* resulting from an anisotropic harmonic model (see text). Both the spherical and the directional distribution along the *c* axis are shown. Bottom panel: the corresponding spherical and directional mean force projected along the *c* axis. The curves are plotted as a function of the end-to-end distance. The mean force enhances the differences between spherical and directional distributions.
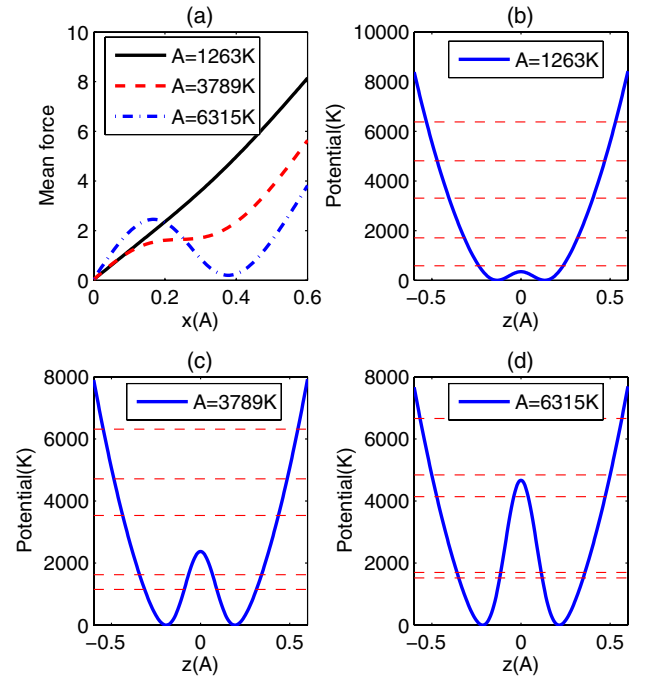

FIG. 3 (color online). (a) The mean force corresponding to a double well model at $T = 30$ K, for different barrier heights $A = 1263$ K (black solid line), $A = 3789$ K (red dashed line), and $A = 6315$ K (blue dot-dashed line). (b) Potential energy surface for $A = 1263$ K (blue solid line), and the first five energy levels (red dashed line). (c),(d) the same as (b), but with $A = 3789$ K and $A = 6315$ K, respectively.
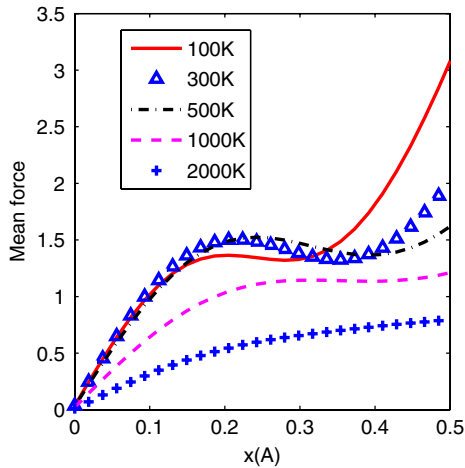
FIG. 4 (color online). The mean force corresponding to a double well model at $A = 3789$ K for different temperatures 100 K (red solid line), 300 K (blue triangle), 500 K (black dot-dashed line), 1000 K (magenta dashed line), and 2000 K (blue cross).

subject to a model double well 1D potential. $V = \frac{m\omega^2}{2} z^2 + A \exp(-\frac{z^2}{2\xi^2})$ with $\omega = 1578$ K, and $\xi = 0.094$ Å. A characterizes the barrier height and is set to be 1263, 3789, and 6315 K, respectively. These parameters mimic different tunneling regimes for protons along a hydrogen bond [5,16]. The temperature is set to be 30 K. At this temperature the behavior of the systems is dominated by the ground state, and the end-to-end distribution can be approximated by the overlap integral $\tilde{n}(x) = \int dz \psi(z) \psi(z + x)$ where $\psi(z)$ is the ground-state wave function and $F(x) = -\frac{d}{dx} \ln \tilde{n}(x)$. In Fig. 3 we can see how qualitatively different the mean force can be in the three cases. One goes from a fully monotonic behavior for $A = 1263$ K which is a model for a low energy barrier hydrogen bond [17], to the strongly nonmonotonic mean forces for $A = 3789$ K, $A = 6315$ K where the tunneling states lie below the barrier height. Additionally, it is not very difficult to relate features of the mean force to the underlying effective potential.

It is also instructive to study $F(x)$ as a function of temperature when the higher states are mixed in the density matrix. This is done in Fig. 4 for the double well potential with $A = 3789$ K. For temperatures in the 100–500 K range, the behavior is dominated by the two lowest eigenstates. The slope of $F(x)$ at small x, which is proportional to the excess kinetic energy K_V, shows little dependence on T. It can be shown with detailed analysis that this is a generic feature of two level tunneling systems. Other characters seen in Fig. 4 in the same range of temperatures, such as the more pronounced kink at intermediate x and the

enhanced softening of the mean force at large x, derive from the odd symmetry of the first excited state contribution. Eventually at higher T the kink in $F(x)$ disappears as the mean force progressively resumes linear behavior with a slope that tends to zero as high temperature classical limit is reached.

In this work, we develop a novel displaced path formalism for the calculation of momentum distribution of quantum particles. The algorithm is rigorous and computationally advantageous. The new formulation introduces in a natural way a potential of mean force which is a quantity that very clearly illuminates the physics behind $n(\mathbf{p})$ and can be used to further understand and analyze experimental and theoretical results.

*Present address: Department of Chemistry, Columbia University, New York, NY 10027, USA.
†rcar@princeton.edu
[1] G. F. Reiter, J. Mayers, and P. Platzman, Phys. Rev. Lett. **89**, 135505 (2002).
[2] G. F. Reiter, J. Li, J. Mayers, T. Abdul-Redah, and P. Platzman, Braz. J. Phys. **34**, 142 (2004).
[3] C. Andreani, D. Colognesi, J. Mayers, G. F. Reiter, and R. Senesi, Adv. Phys. **54**, 377 (2005).
[4] J. A. Morrone and R. Car, Phys. Rev. Lett. **101**, 017801 (2008).
[5] J. A. Morrone, L. Lin, and R. Car, J. Chem. Phys. **130**, 204511 (2009).
[6] D. Ceperley, Rev. Mod. Phys. **67**, 279 (1995).
[7] D. Ceperley and E. Pollock, Can. J. Phys. **65**, 1416 (1987).
[8] J. A. Morrone, V. Srinivasan, D. Sebastiani, and R. Car, J. Chem. Phys. **126**, 234504 (2007).
[9] See supplementary material at http://link.aps.org/supplemental/10.1103/PhysRevLett.105.110602 for the derivation of (3) and (6).
[10] M. Herman, E. Bruskin, and B. Berne, J. Chem. Phys. **76**, 5150 (1982).
[11] R. W. Zwanzig, J. Chem. Phys. **22**, 1420 (1954).
[12] J. Kirkwood, J. Chem. Phys.. **3**, 300 (1935).
[13] J. Lobaugh and G. A. Voth, J. Chem. Phys. **106**, 2400 (1997).
[14] L. Lin, J. A. Morrone, R. Car, and M. Parrinello (to be published).
[15] A. Pietropaolo, R. Senesi, C. Andreani, A. Botti, M. A. Ricci, and F. Bruni, Phys. Rev. Lett. **100**, 127802 (2008).
[16] M. Benoit, D. Marx, and M. Parrinello, Nature (London) **392**, 258 (1998).
[17] M. Benoit and D. Marx, Chem. Phys. Chem. **6**, 1738 (2005).